Persistent current of atoms in a ring optical lattice

Andrey R. Kolovsky[1,2]

[1]Max-Planck-Institut für Physik komplexer Systeme, 01187 Dresden, Germany
[2]Kirensky Institute of Physics, 660036 Krasnoyarsk, Russia

E-mail: kolovsky@mpipks-dresden.mpg.de

Abstract. We consider a small ensemble of Bose atoms in a ring optical lattice with weak disorder. The atoms are assumed to be initially prepared in a superfluid state with non-zero quasimomentum and, hence, may carry matter current. It is found that the atomic current persists in time for a low value of the quasimomentum but decays exponentially for a high (around one quater of the Brillouin zone) quasimomentum. The explanation is given in terms of low- and high-energy spectra of the Bose-Hubbard model, which we describe using the Bogoliubov and random matrix theories, respectively.

1. Introduction

Ultracold atoms in optical lattices constitute an intense research activity both in experimental and theoretical physics. Up to now this system has mostly been used for modelling the fundamental Hamiltonians of solid state theory (see, [1, 2], for example) where the number of particles is macroscopically large. However, the recent progress with manipulating a countable number of atoms [3, 4] makes it possible to build a system of arbitrary size, ranging from microscopic to macroscopic. In this border region between microscopic and macroscopic one has to deal with a finite number of atoms which, on the one hand, is too large to use the single-particle approach but, on the other hand, is too small to justify the thermodynamic limit. In the present work we theoretically analyse one of these problem related to superfluidity of a few ($N \sim 10$) Bose atoms in a ring optical lattice [5] with a few ($L \sim 10$) sites.

It should be stressed in the very beginning that, currently, there are two different definitions of superfluidity in the physics literature. One definition is based on the system's responce to a phase twist. With respect to Bose atoms in a lattice this approach is discussed, in particular, in Ref. [6], and a method of how one can realize the twisted boundary conditions in a laboratory experiment is suggested in Ref. [5]. The other definition originates in the Landau criterion of superfluidity and involves a responce of a superfluid flow to 'wall roughness' [7, 8]. In this work we try to reconcile both approaches. Specifically, we address the following problem. Assume that we have N Bose atoms in a ring lattice with L sites in a superfluid state with given quasimomentum $\kappa = 2\pi k/L$:

$$|\kappa\rangle = \left(\frac{1}{\sqrt{L}} \sum_l \hat{a}_l^\dagger e^{i\kappa l}\right)^N |0\rangle \ . \tag{1}$$

We are interested in the time evolution of this state (which we also shall refer to as the supercurrent state) in the presence of a weak scattering potential and atom-atom interactions.

We note that for a BEC of atoms ($N \gg 1$) the problem of superfluid atomic current has been considered in a large number of papers (see Refs. [9, 10, 11, 12, 13, 14, 15, 16], to cite few of them). The starting point of all these studies is the mean-field approach, which is sometimes rectified by taking into account the quantum fluctuations [15, 16]. The mean-field theory predicts a destruction of the supercurrent as soon as the quasimomentum exceeds one quater of the reciprocal lattice constant ($\kappa > \pi/2$ in the notations used). In order to justify the mean-field approach in a 1D lattice the mean number of atoms per one site should be much larger than unity. As stated above, in the present work we focus on the opposite limit $N/L \sim 1$, where the mean-field approach is not applicable. For this reason we treat cold atoms in an optical lattice from a different viewpoint, in a sense closer to quantum optics than to condensed matter physics.

The paper essentially consists of two parts, – in the first part (Sec. 2), after a brief preliminary analysis, we report the results of numerical simulations of the system dynamics, and in the second part (Sec. 3 and Sec. 4) we explain the observed regimes

in terms of the energy spectrum of the system. The main results are summarized in the concluding Sec. 5.

2. Supercurrent dynamics

Before proceeding with numerical simulations, we shall briefly discuss possible regimes for the atomic current.

2.1. Preliminary analysis

Let us first consider the single-particle problem. In the tight-binding approximation the Hamiltonian of the system reads

$$\widehat{H} = -\frac{J}{2}\sum_l (|l+1\rangle\langle l| + h.c.) + \sum_l V_l |l\rangle\langle l| \; , \tag{2}$$

where $|l\rangle$ are the Wannier functions, J the hopping matrix element, and V_l the random scattering potential. In what follows, to be concrete, we shall consider $0 \leq V_l \leq \epsilon$ with $\epsilon \ll J$. The operator $\widehat{V} = \sum_l V_l |l\rangle\langle l|$ couples the degenerate states with opposite quasimomentum, resulting in new eigenstates $|\kappa_{c,s}\rangle = (|\kappa\rangle \pm |-\kappa\rangle)/\sqrt{2}$ with an energy splitting $|E_c - E_s| = 2|\langle\kappa|\widehat{V}|-\kappa\rangle| = 2|V(2k)|$, where

$$V(k) = \frac{1}{L}\sum_l V_l \exp\left(\frac{2\pi k}{L} l\right) \sim \frac{\epsilon}{L}$$

is the Fourier transform of V_l. Thus, in course of time, an atom in a ring will periodically change its momentum to the opposite one with the frequency $\Omega_\epsilon \sim \epsilon/\hbar L$. It is worth of stressing that this periodic dynamics is exclusively due to the finiteness of L and the assumed condition $\epsilon \ll J$, which means that $\widehat{V}$ couples only the degenerate states of the unperturbed system. ‡

Next we consider the multi-particle case,

$$\widehat{H} = -\frac{J}{2}\sum_l \left(\hat{a}_{l+1}^\dagger \hat{a}_l + h.c.\right) + \frac{U}{2}\sum_l \hat{n}_l(\hat{n}_l - 1) + \sum_l V_l \hat{n}_l \; , \tag{3}$$

where $\hat{a}_l^\dagger$ and $\hat{a}_l$ are the bosonic creation and annihilation operator, $\hat{n}_l = \hat{a}_l^\dagger \hat{a}_l$, and U is the on-site interaction energy. Using the canonical transformation, $\hat{b}_k = (1/\sqrt{L})\sum_l \exp(i2\pi kl/L)\hat{a}_l$, it is convenient to present the Hamiltonian (3) in the form

$$\widehat{H} = -J\sum_k \cos\left(\frac{2\pi k}{L}\right)\hat{b}_k^\dagger \hat{b}_k + \frac{U}{2L}\sum_{k_1,k_2,k_3,k_4} \hat{b}_{k_1}^\dagger \hat{b}_{k_2}^\dagger \hat{b}_{k_3}\hat{b}_{k_4}\tilde{\delta}(k_1+k_2-k_3-k_4)$$
$$+ \sum_{k_1,k_2} V(k_1-k_2)\hat{b}_{k_1}^\dagger \hat{b}_{k_2} \; , \tag{4}$$

where $\tilde{\delta}(k) = 1$ if k is a multiple of L, and $\tilde{\delta}(k) = 0$ otherwise. For $U = 0$ and $\epsilon = 0$ the multi-particle eigenstates of the system (4) are the quasimomentum Fock

‡ In terms of Anderson's localization theory the above conditions mean that the Anderson localization length is much larger than the system size.

states $|\mathbf{n}\rangle = |n_0, n_1, \ldots, n_{L-1}\rangle$, where $\sum_k n_k = N$. Our state of interest corresponds to $|\kappa\rangle = |\ldots, 0, N_k, 0, \ldots\rangle$, where all atoms have one and the same quasimomentum. Similar to the single-particle case, the random potential couples this state to the supercurrent state with the opposite quasimomentum $|-\kappa\rangle = |\ldots, 0, N_{k'}, 0, \ldots\rangle$, $k' = \mathrm{mod}_L(-k)$. However, now the coupling is indirect and involves the intermidiate states $|\kappa(m)\rangle = |\ldots, (N-m)_k, \ldots, m_{k'}, \ldots\rangle$, as it immediately follows from the explicit form of the scattering potential in the momentum representation. Thus the time evolution of the state $|\kappa\rangle$ is defined by the following $(N+1)\times(N+1)$ matrix,

$$A_{m,m'} = E_m\delta_{m,m'} + \sqrt{(N-m)(m+1)}\,[V(2k)\delta_{m+1,m'} + V^*(2k)\delta_{m,m'+1}] \ , \quad (5)$$

where $E_m = E_\kappa \equiv -JN\cos\kappa$ are the degenerate energies of the states $|\kappa(m)\rangle$ and the next terms the transition matrix elements $\langle\kappa(m)|\widehat{V}|\kappa(m')\rangle$. The spectrum of the matrix (5) is equidistant with the level spacing $2|V(2k)|$. Thus we have reproduced the result of the single-particle analysis, where the time evolution of the system is periodic with the frequency $\Omega_\epsilon \sim \epsilon/\hbar L$.

Now we switch on the interaction. Then the intermidiate states $|\kappa(m)\rangle$ aquire energy shifts $E_m = E_m(U)$, which appear to be m-dependent. Using the first order perturbation theory we obtain

$$\begin{aligned} E_m &= E_\kappa + \frac{U}{2L}\langle\kappa(m)|\sum \hat{b}^\dagger_{k_1}\hat{b}^\dagger_{k_2}\hat{b}_{k_3}\hat{b}_{k_4}\tilde{\delta}(k_1+k_2-k_3-k_4)|\kappa(m)\rangle \\ &= E_\kappa + \frac{U}{2L}\left[(N-m)(N-m-1) + m(m-1) + 4(N-m)m\right] \\ &\approx E_\kappa + \frac{UN^2}{2L} + \frac{U}{L}m(N-m) \ . \end{aligned} \quad (6)$$

Due to the mismatch of the energy levels E_m, the supercurrent states $|\kappa\rangle \equiv |\kappa(0)\rangle$ and $|-\kappa\rangle \equiv |\kappa(N)\rangle$ become effectively decoupled and, hence, the supercurrent should persist in time.

At this point we would like to note the analogy of the problem discussed with that for a BEC in double well potential [17]. Drawing this analogy further we can estimate the minimal U_{min} required for stabilization of the suppercurrent as

$$U_{min} \approx 8\epsilon/N \ . \quad (7)$$

For the sake of completeness we present a derivation of the estimate (7) in the next subsection (which can be safely skipped if a reader is familiar with the subject).

2.2. Semiclassical approach

The standart method of treating the system (5-6) consist of mapping it onto an effective classical system (terms proportional to the identity matrix are omitted),

$$H_{eff} = gI(1-I) + 2|V|\sqrt{I(1-I)}\cos\theta \ , \quad g = UN/L \ , \quad (8)$$

followed by a semiclassical quantization, where $1/N$ plays the role of Planck's constant. The phase portrait of the system (8) is shown in Fig. 1 for $g/|V| = 1$ and $g/|V| = 10$. It

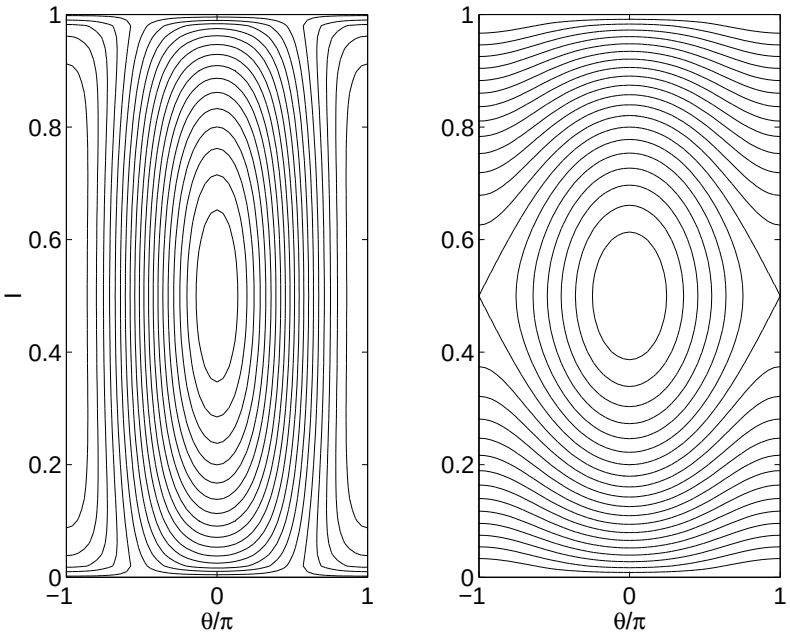

Figure 1. Phase portrait of the effective system (8) for $g/|V| = 1$ (left panel) and $g/|V| = 10$ (right panel).

is seen that when g is increased the phase portrait becomes similar to that of classical pendulum, with a separatrix separating the librational and rotational regimes. The maximal and minimal values of the classical action I along the separatrix are given by $I^* \approx 1/2 \pm \sqrt{|V|/2g}$. The quantum states, associated with I, are decoupled only if they lie above the separatrix. Then, by requiring $|I^* - 1/2| \leq 1/2$ and noting that $|V| \sim \epsilon/L$, we come to the estimate (7).

Needless to say, the semiclassical approach described above requires $1/N \ll 1$ and is not accurate for small N. Nevetheless, even for $N \sim 10$ the spectrum of the matrix A can be well understood in terms of the effective system (8). For the purpose of future reference, the right panel in Fig. 2 shows the numerical solution of the matrix eigenvalue problem for $N = 7$, $L = 9$, and $|V| = 0.0168$. In particular, at $U = 0.2J$ one can identify the first four top levels with the phase trajectories below the separatrix, next two levels with trajectories around the separatrix, and the last two almost degenerate levels with trajectories well above the separatrix.

2.3. Numerical results

The above conclusion about the persistent current relies on the applicability of a perturbative approach. Formally this means that the supercurrent state $|\kappa\rangle$, as well as the intermidiate states $|\kappa(m)\rangle$, have to be approximate eigenstates of the system at $\epsilon = 0$. This imposes the upper boundary U_{max} on the interaction constant, which appears to depend on the quasimomentum κ. Indeed, the state $|\kappa\rangle$ with the energy $E_\kappa \approx -JN \cos\kappa$ is an approximate eigenstate of the system only if U is smaller than

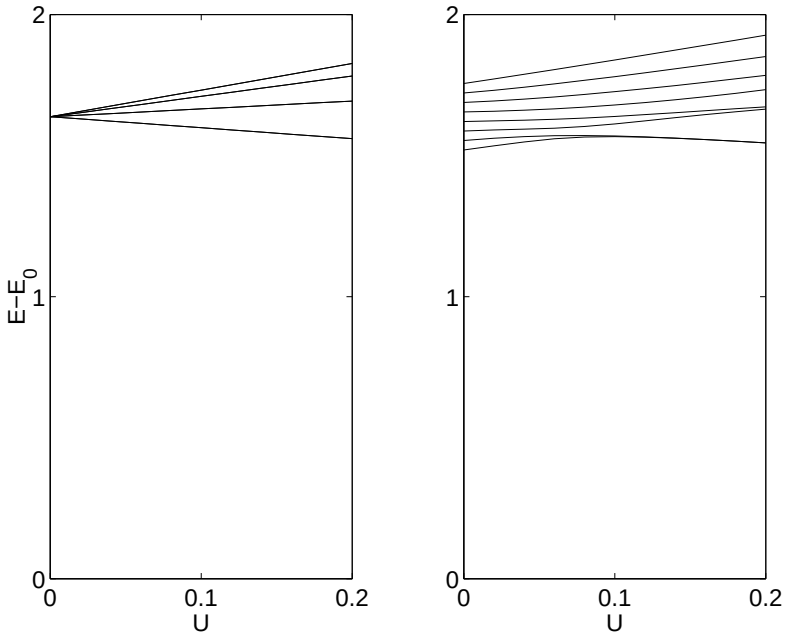

Figure 2. Spectrum of the matrix (5-6) as function of the interaction constant U. (The energy is measured in units of J, $E_0 = -JN + UN^2/2L$.) Parameters are $N = 7$, $L = 9$, $\kappa = 2\pi/L$, and $|V(2)| = 0$ (left panel) and $|V(2)| = 0.0168$ (right panel).

the characteristic energy gap separating it from the other energy states, coupled to $|\kappa\rangle$ by interaction. As the first guess one can set this gap to the mean level spacing, given by the inverse density of state $\overline{\Delta E} = 1/f(E)$. It is easy to show that for $U/J \leq 1$ the density of states of (3) is given by the Gaussian distribution (see Fig. 4 below)

$$f(E) \approx \frac{\mathcal{N}}{\sqrt{2\pi}\sigma} \exp\left[\frac{(E-\bar{E})^2}{2\sigma^2}\right] , \tag{9}$$

where $\mathcal{N} = (N+M-1)!/N!(M-1)!$ is the dimension of the Hilbert space, $\sigma \sim J\sqrt{N}$ and $\bar{E} \sim UN^2/L + \epsilon N/2$. Thus the characteristic gap for a supercurrent state, which belongs to the central part of the spectrum (i.e., for $\kappa \sim \pi/2$), is essentially smaller than that for a supercurrent state with low quasimomentum $\kappa \ll \pi/2$. As a consequence, U_{max} for the supercurrent state with $\kappa \sim \pi/2$ may be smaller than U_{min}. In the other words, the perturbative approach of Sec. 2.1 (where we used first order perturbation theory to find corrections to the eigenenergies of states $|\kappa(m)\rangle$) breaks down before the stabilization of the supercurrent is achieved.

Figure 3 compares the dynamics of $N = 7$ atoms in a lattice with $L = 9$ sites, which were initially prepared in the supercurrent state (1) with high, $\kappa = 6\pi/L$, and low, $\kappa = 2\pi/L$, quasimomentum. The normalized mean momentum of the atoms, $p(t) = N^{-1}\mathrm{Im}[\langle\Psi(t)|\sum_l \hat{a}^\dagger_{l+1}\hat{a}_l|\Psi(t)\rangle]$, is depicted. It is seen in the upper panel of Fig. 3 that in the former case of high quasimomentum the oscillatory behaviour of $p(t)$ changes to irreversible decay as the interaction constant is varied from $U = 0.02$ to $U = 0.2$. (From now on we set $J = 1$, i.e., energy is measured in the units of J and time in the units $T = 2\pi\hbar/J$.) Further increase of the interaction constant (results are not shown)

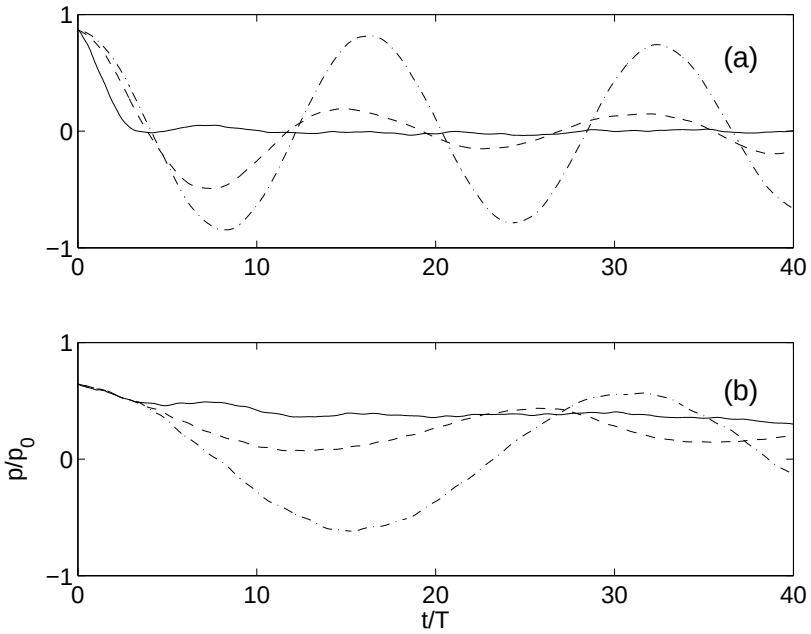

Figure 3. The mean momentum of $N = 7$ atoms in a lattice with $L = 9$ sites. The magnitude of the scattering potential $\epsilon = 0.2$. The interaction constant $U = 0.02$ (dash-dotted lines), $U = 0.1$ (dashed lines), and $U = 0.2$ (solid lines). The atoms are initially prepared in the supercurrent state (1) with $\kappa = 6\pi/L$ (upper panel) and $\kappa = 2\pi/L$ (lower panel).

is reflected in even faster decay of $p(t)$. This should be contrasted with the case of low quasimomentum (lower panel), where the current oscillations at $U = 0.02$ change to persistent current at $U = 0.2$. Here further increase of U leaves the system dynamics qualitatively unchanged at least till $U = 1$. The displayed numerical results suggest that the perturbative approach of Sec. 2.1 works for $\kappa = 2\pi/L$ but does not work for $\kappa > 2\pi/L$. We shall come back to this point later on in Sec. 4.3.

It is worth stressing that through the paper we consider a single realization for the random potential (i.e., no average over disorder). Specifically to the considered lattice of $L = 9$ sites, the random entries are $V_l = \epsilon(0.80, 0.59, 0.06, 0.18, 0.97, 0.31, 0.67, 0.78, 0.49)$. The Fourier transform of this sequence gives $|V(2k)| = 0.084\epsilon$ and $|V(2k)| = 0.144\epsilon$ for $k = 1$ and $k = 3$, respectively.

3. High-energy spectrum

To get a better insight in the physics of the discussed phenomena we shall discuss the displayed in Fig. 3 results in terms of the energy spectrum of the system (3). We begin with the case of a high quasimomentum which, as mentioned above, refers to the central part of the spectrum.

3.1. Spectral statistics

We have found that in the case of high initial quasimomentum a transition from oscillatory dynamics to irreversible decay is associated with the transition to chaos in the Bose-Hubbard model. Following Ref. [19], we shall monitor this transition by analysing the distribution of distances between the neighbouring levels, normalised to the mean level spacing: $s = (E_{n+1} - E_n)/\overline{\Delta E} = (E_{n+1} - E_n) f[(E_{n+1} + E_n)/2]$. It should be stressed that the presence of random potential in the Hamiltonian (3) alone does not yet induced chaos in the system. The only consequence of a weak disorder (relevant to the spectral statistics) is that it breaks the translational symmetry and, hence, we need not worry about decomposition of the energy spectrum into the independent subsets (labeled, in the absence of a random potential, by total quasimomentum of the atoms [19]).

The results of the statistical analysis of the high-energy spectrum are presented in Fig. 4. The dash-dotted and dashed lines in panel (c) correspond to the integrated distribution, $I(s) = \int_0^s P(s')ds'$, for the Poisson statistics,

$$P(s) = \exp(-s) \ , \tag{10}$$

which is typical for a generic integrable system, and the Wigner-Dyson statistics,

$$P(s) = \frac{\pi}{2} s \exp\left(-\frac{\pi}{4} s^2\right) \ , \tag{11}$$

typical for non-integrable systems. These distributions reflect the different character of the parametric dependence of the energy levels $E_n = E_n(\lambda)$ on some parameter in the Hamiltonian ($\lambda = U$ in our case). Namely, in the integrable case the energy levels may cross and, hence, one finds an arbitrary small s. On the contrary, if the system is non-integrable, the energy levels show avoided crossings and probability of finding small s tends to zero.

The panel (a) in Fig. 4 shows the density of states $f(E)$ for $U = 0.02$, where only the data from the central part of the spectrum (marked by the inverse parabola) were used for the statistical analysis. It is seen in the lower panel that for $U = 0.02$ the level spacing distribution follows the Poisson statistics. Thus for this value of the interaction constant the system should be classified as integrable, which is consistent with the periodic dynamics of the mean momentum in Fig. 3(a). The panel (b) in Fig. 4 shows the density of states for $U = 0.2$. Apart from an uniform shift of the spectrum to positive values, no qualitative change in $f(E)$ is observed. However, we do observe a qualitative change in the level spacing distribution. Now it reliably follows the Wigner-Dyson statistics which, as mentioned above, is a hallmark of quantum chaos.

3.2. Local density of states

The spectral statistics is only one (and, in fact, rather poor) characteristic of the system. In particular, the level spacing distribution remains unchanged (Wigner-Dyson) in the interval $0.2 \leq U \leq 1$, although the decay rate of the supercurrent changes with U. One

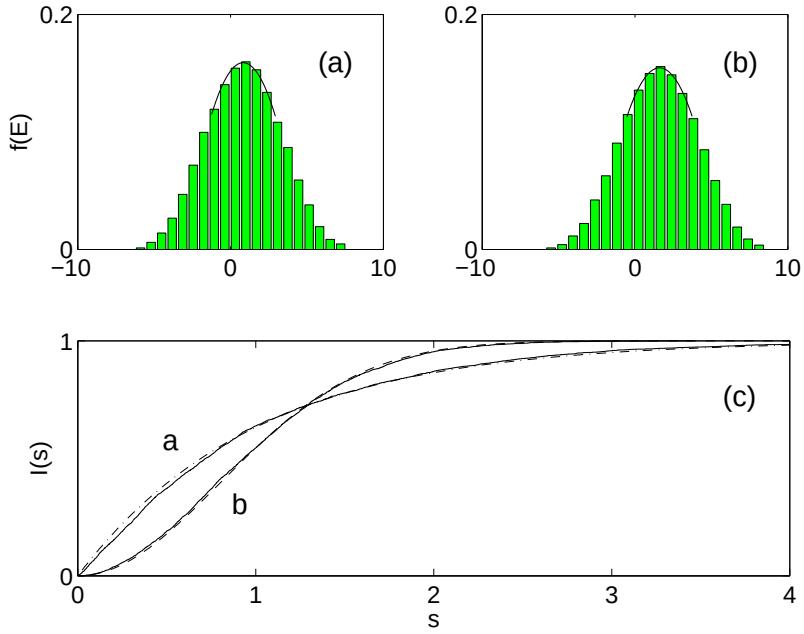

Figure 4. (a,b) – density of states of $N = 7$ atoms in a lattice with $L = 9$ sites for the interaction constant $U = 0.02$ and $U = 0.2$, respectively. The magnitude of the scattering potential $\epsilon = 0.2$. (c) – integrated level spacing distributions for the central part of the spectrum.

gets more information about the system by studying its eigenfunctions. To this end we introduce a quantity $R(m, n)$,

$$R(m, n) = |\langle \Psi_m(U')|\Psi_n(U)\rangle|^2 \,, \tag{12}$$

closely related to the so-called local density of states. § In Eq. (12) $|\Psi_n(U)\rangle$ are the eigenfunctions of the Hamiltonian (3) calculated for a given U and ordered according to their energies. In what follows we shall fix $U' = 0.02$ while U will be scanned in the interval $0.2 \leq U \leq 1$. Since for $U = 0.02$ the system is integrable, the matrix (12) can be alternatively viewed as the matrix of the expansion coefficients of the chaotic states $|\Psi_n(U)\rangle$ over 'regular basis' $|m\rangle = |\Psi_m(U = 0.02)\rangle$.

The characteristic structure of the matrix (12) is shown in Fig. 5 for $U = 0.2$. It is seen that that R is a banded matrix with strongly fluctuating matrix elements. The mean values of the elements across the main diagonal,

$$\bar{R}(\Delta m) = \frac{1}{M} \sum_{m=-M/2}^{M/2} R(m, m + \Delta m) \,, \quad \sum_{\Delta m} \bar{R}(\Delta m) = 1 \,, \tag{13}$$

are shown in Fig. 6 on linear and logarithmic scales. (Here, as in the spectrum analysis, we consider an energy window of the order of unity in the central part of the spectrum.)

§ The local density of states is defined as $R(m, E) = \sum_n R(m, n)\delta(E - E_n)$.

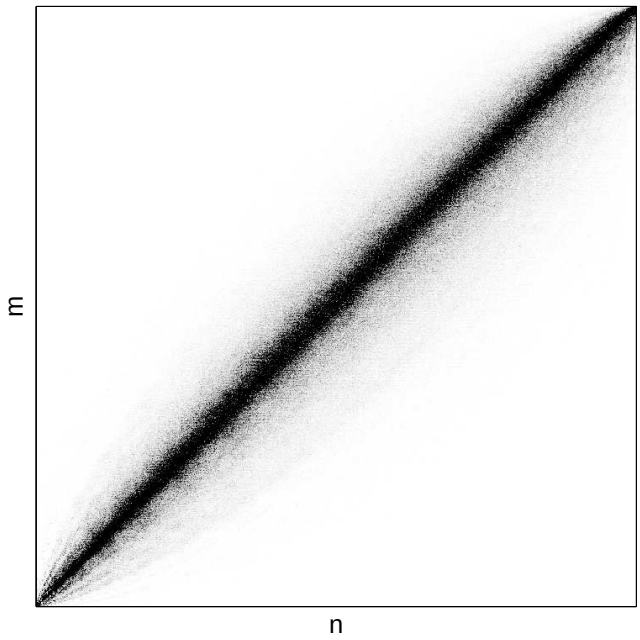

Figure 5. Gray-scale image of the matrix (12). (The system parameters are the same as in Fig. 3 and Fig. 4.)

It is seen that $\bar{R}(\Delta m)$ converges to the Lorentzian, ‖

$$\bar{R}(\Delta m) = \frac{\Gamma/2\pi}{(\Delta m)^2 + \Gamma^2/4} \,. \tag{14}$$

We note, in passing, that a similar result is reported in the recent paper [21] devoted to the spectral properties of the three-site Bose-Hubbard model.

The distribution (14), also known as the Breit-Wigner formula, implies the exponential decay of the supercurrent state. Indeed, considering the overlap integral $\langle\kappa|\kappa(t)\rangle$, one has

$$\begin{aligned}\langle\kappa|\exp\left(-\frac{i}{\hbar}\widehat{H}t\right)|\kappa\rangle &= \sum_{m,m',n}\langle\kappa|m\rangle\langle m|\Psi_n\rangle\exp\left(-\frac{i}{\hbar}E_n t\right)\langle\Psi_n|m'\rangle\langle m'|\kappa\rangle \\ &\approx \frac{1}{N+1}\sum_m R(m,n)\exp\left(-\frac{i}{\hbar}E_n t\right) \sim \sum_{\Delta m}\bar{R}(\Delta m)\exp\left(-\frac{i\overline{\Delta E}t}{\hbar}\Delta m\right) \,,\end{aligned}$$

where we substitute the exact energy levels E_n by their approximate positions, $E_n \approx E_\kappa + \overline{\Delta E}\Delta m$. (This approximation obviously holds till time $t_\hbar \sim \hbar/\overline{\Delta E} = \hbar f(E_k)$, which increases exponentially with the system size.) Substituting here $\bar{R}(\Delta m)$ from Eq. (14) we have $\langle\kappa|\kappa(t)\rangle = \exp(-\Gamma\overline{\Delta E}t/\hbar)$. We found that the width Γ grows approximately quadratically with U in the interval $0.2 \le U \le 1$.

‖ The distribution (14) is typical for the banded random matrices [20]. It is interesting to note in this connection that for the $N/L \sim 1$ neither matrix of the Hamiltonian (3) nor that of the Hamiltonian (4) are banded. It is an open problem in the random matrix theory to extend the results of [20] to the present case of very sparse but not banded matrices.

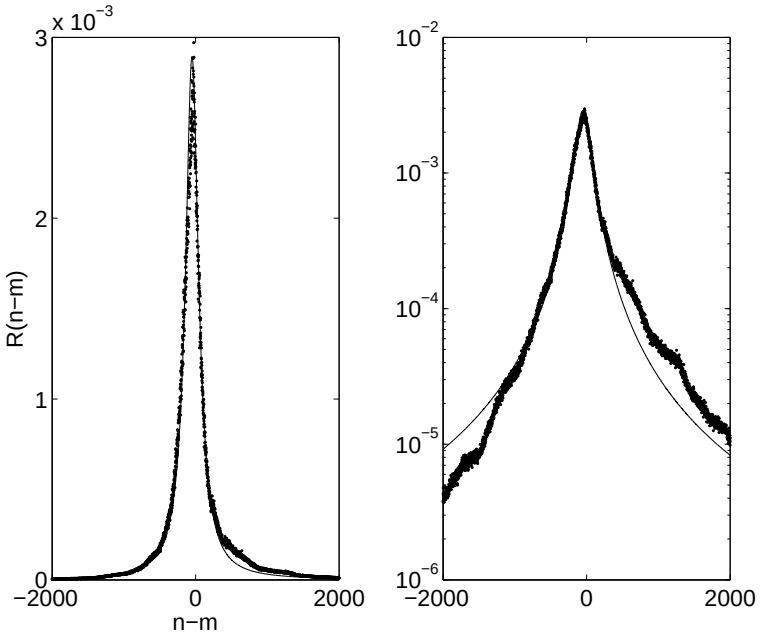

Figure 6. Mean values of the matrix elements across the main diagonal in the central part of the matrix. The solid line is the best fit by the Breit-Wigner formula (14).

4. Low-energy spectrum

We turn to the case of low quasimomentum. For small κ the energy of the supercurrent state (1) falls into the low-energy tail of the density of states (9), where the random matrix approach is not applicable. On the other hand, the low-energy spectrum of the interacting Bose atoms is believed to be described by the Bogoliubov theory. For this reason we review the Bogoliubov approach for a finite size system. Through the section, if not stated otherwise, we assume the homogeneous case $\epsilon = 0$.

4.1. Bogoliubov approach

As an intermidiate step, let us show that the Bogoliubov approach amounts to the following two assumptions. (i) The low energy eigenstates of interacting Bose atoms are given by a linear superposition of the quasimomentum Fock states, where n atoms have quasimomentum κ, n quasimomentum $-\kappa$, and the rest $N - 2n$ have zero quasimomentum [18], i.e.,

$$|\Psi_\kappa\rangle = \sum_{n=0}^{N/2} c_n |N-2n, \ldots, n_k, \ldots, n'_k, \ldots, 0\rangle \ , \quad k' = \mathrm{mod}_L(-k) \ . \tag{15}$$

(ii) The number of atoms with $\kappa \neq 0$ is small compared to the number of atoms with zero quasimomentum, i.e., only the coefficients c_n with $n \ll N/2$ have non-negligible values. (This condition is automatically satisfied if one assumes the thermodynamic limit $N \to \infty$, $U \to 0$, $UN = const.$)

The analysis goes as follows. Substituting the wave function (15) in the eigenvalue equation with the Hamiltonian (4), we get a system of linear equations for the coefficients c_n,

$$(2E_k n + \frac{U}{L}a_n)c_n + \frac{U}{L}(b_n c_{n-1} + b_{n+1}c_{n+1}) = Ec_n \ , \tag{16}$$

where

$$a_n = 2nN - 3n^2 + n + N(N-1)/2 \approx n(2N-3n) + N^2/2 \ ,$$
$$b_n = (n+1)\sqrt{(N-2n)(N-2n-1)} \approx n(N-2n) \ ,$$

and $E_k = J[1-\cos(2\pi k/L)]$ is the single-particle excitation energy (should not be missmatched with the energy of the supercurrent state, $E_\kappa = -JN\cos\kappa$). Assuming the thermodynamic limit, Eq. (16) simplifies to

$$2(E_k+g)nc_n + gnc_{n-1} + g(n+1)c_{n+1} = Ec_n \ , \quad g = NU/L \ . \tag{17}$$

Next, introducing the generating function,

$$\Phi(\theta) = \frac{1}{\sqrt{2\pi}}\sum_{n=-\infty}^{\infty} c_n e^{in\theta} \ ,$$

we present the system of linear equations (17) as a differential equation on the function $\Phi(\theta)$, ¶

$$g\left[\hat{n}e^{i\theta} + 2(1+\epsilon)\hat{n} + e^{-i\theta}\hat{n}\right]\Phi(\theta) = E\Phi(\theta) \ , \tag{18}$$

where $\hat{n} = -i\partial/\partial\theta$ and $\varepsilon = E_k/g$. The general solution of (18) reads

$$\Phi(\theta) = C\exp\left(i\int_0^\theta \frac{E/g - e^{i\vartheta}}{2\cos\vartheta + 2 + \varepsilon}d\vartheta\right) \ . \tag{19}$$

Finally, requiring $\Phi(\theta+2\pi) = \Phi(\theta)$ and calculating the relevant integral,

$$\frac{1}{2\pi}\int_0^{2\pi}\frac{d\theta}{2\cos\theta + 2 + \varepsilon} = \frac{1}{2\sqrt{(1+\varepsilon)^2 - 1}} \ ,$$

we get the equidistant spectrum with the transition frequency

$$\omega_k = 2\sqrt{2gE_k + E_k^2} \ . \tag{20}$$

The result (20) reproduces the famous Bogoliubov equation for the quasiparticle excitations of the Bogoliubov vacuum.

4.2. Bogoliubov spectrum

In the previous subsection we have considered an excitation of the given quasimomentum state, with the single-particle excitation energy $E_k = J(1-\cos\kappa)$. To include the other quasimomentum states, the ansatz (15) should be generalized to

$$|\Psi\rangle = \sum_{\mathbf{n}} c_{\mathbf{n}}|N - 2\sum_k n_k, n_1, n_2, \ldots\rangle \ , \tag{21}$$

¶ To be regorous, Eq. (18) is not strictly equivalent to Eq. (17) in the sense that it also has solutions with negative E.

where $\mathbf{n} = (n_1, \ldots, n_{L/2})$. Substituting (21) in the stationary Schrödinger equation with the Hamiltonian (4), we obtain a system of rather complex equations on the coefficients $c_{\mathbf{n}}$, which can be solved analytically only in the thermodynamic limit. In this limit, as it is easy to show, the whole eigenvalue problem factorizes to $L/2$ eigenvalue problems of the form (17) and, hence, the whole spectrum is given by the direct sum of $L/2$ linear spectra.

A remark about the total quasimomentum, which is a global symmetry of the system in the absence of random potential, is in turn. The substitution (15) corresponds to zero total quasimomentum. To get non-zero values of the total quasimomentum, one should use a slightly different ansatz,

$$|\Psi_\kappa\rangle = \sum_{n=0}^{N/2} c_n |N-2n-m, \ldots, n_k+m, \ldots, n'_k, \ldots, 0\rangle \ , \qquad (22)$$
$$k' = \mathrm{mod}_L(-k) \ , \quad m = 1, \ldots, L-1 \ .$$

Ansatz (22) leads to the eigenvalue equation of the form (16) but with different coefficients a_n and b_n. In particular, considering the thermodynamic limit, Eq. (17) changes to

$$2(E_k+g)(n+m)c_n + g\sqrt{n(n+m)}c_{n-1} + g\sqrt{(n+1)(n+m+1)}c_{n+1} = Ec_n \ . \qquad (23)$$

We note, in passing, that if the spectra associated with different single-particle excitation energy and different total quasimomentum are superimposed,

$$E = \sum_{k,m} \left\{ E^{(k,m)}(g) \right\} \ , \qquad (24)$$

one typically finds a multiple degeneracy of the levels at $U = 0$ (see Fig. 8 below).

It is interesting to compare the discussed Bogoliubov spectrum of an infinite system with the low-energy spectrum of a finite system. For this reason we calculate numerically the spectrum of $N = 25$ atoms in a lattice with $L = 5$ sites. [+] A few first levels of this system are depicted in the left panel of Fig. 7 where, to facilitate a comparison, we substract the energy $E_0 = -JN + UN(N-1)/2L$ and rescale energy axis on the basis of the frequency $\omega_1 = \omega_1(U)$. The Bogoliubov spectrum, calculated by using Eqs. (23-24), is depicted in the right panel of Fig. 7. Both similarities and differences are evident. The first two levels are seen to coincide in the whole interval $0 \le U \le 1$. On the other hand, multiple degeneracy of the levels around $U = 0.13$ in the right panel is removed in the left panel. This is, in fact, not surprising. Indeed, let us consider the lowest group of levels, showing the degeneracy. These levels are associated with the qusimomentum Fock states $|0, 2, 21, 2, 0\rangle$, $|0, 2, 22, 0, 1\rangle$, $|1, 0, 22, 2, 0\rangle$, and $|1, 0, 23, 0, 1\rangle$. (Here we use a different notation for the Fock states, corresponding to the Brillouin zone $-\pi < \kappa \le \pi$.) These states belong to different spectra, labeled by k and m in Eq. (23), and are decoupled within the Bogolubov approach. However, for the considered finite system these states are coupled by interaction, where the coupling matrix elements are of the order of g/N.

[+] For $L = 5$ there are two different frequencies ω_k. In this sense, $L = 5$ is the simplest generic case to discuss the Bogoliubov spectrum.

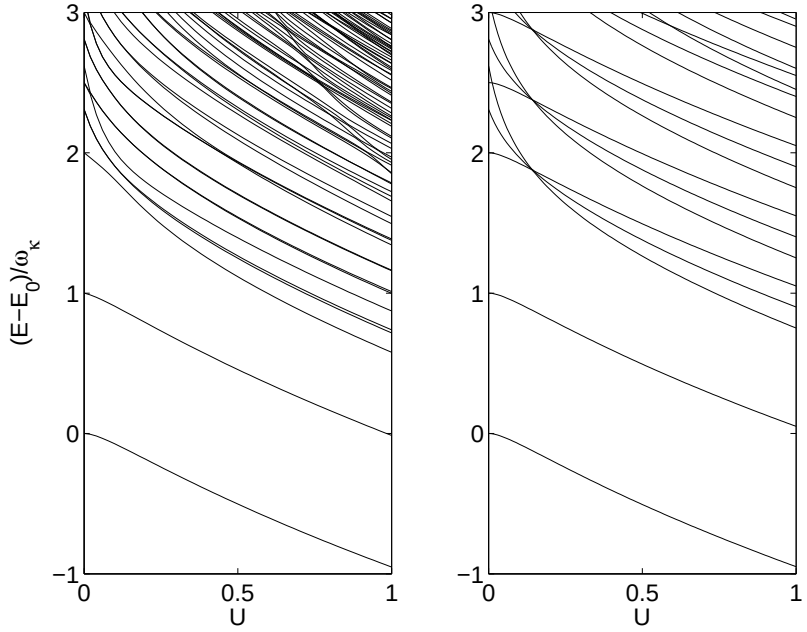

Figure 7. Left panel: first few energy levels of $N = 25$ atoms in a lattice with $L = 5$ sites, as function of the on-site interaction constant. (Only the levels corresponding to zero total quasimomentum are shown.) Right panel: first few energy levels of the Bogoliubov spectrum, calculated on the basis of Eq. (23) and Eq. (24).

4.3. Persistent current

In this subsection we critically review the result of Sec. 2 about the persistent current, carefully checking validity of the perturbative approach. Left panel in Fig. 8 shows the low-energy levels for $N = 7$ and $L = 9$ (whole spectrum is shown, i.e., no symmetry selection according to the total quasimomentum). Remarkably, even for such a small number of atoms one still has a qualitative agreement with the Bogoliubov spectrum. Our states of interest in Fig. 8 are the supercurrent and the intermidiate states $|\kappa(m)\rangle$, which originate from the point marked by an asterisk. It is seen, by comparing with Fig. 2(a), that (i) the splitting between these levels well matches Eq. (5) and (ii) the coupling of these states to the other states of the system is negligible, which is indicated by absence of the avoided crossings. In addition to the case $\epsilon = 0$, right panel in Fig. 8 shows the spectrum of the atoms in the presence of a weak scattering potential [should be compared with Fig. 2(b)]. Again, no avoided crossings with the other levels are seen. Hence, the approach of Sec. 2 is well justified.

The above visual analysis of the spectrum can be made quantitative by considering the overlap of the supercurrent state $|\kappa\rangle$ with the exact eigenstates,

$$Q(U) = \max_{n=1}^{\mathcal{N}} \left(|\langle \kappa | \Psi_n(U) \rangle|^2 \right) \ . \tag{25}$$

For $\kappa = 0$ the quantity (25) is obviously maximazed by the ground state $|\Psi_0(U)\rangle$, which is expected to coincide with the Bogoliubov state ground. The solid line in Fig. 9 shows the overlap of the state $|\kappa = 0\rangle$ with the ground Bogoliubov state. A monotonic

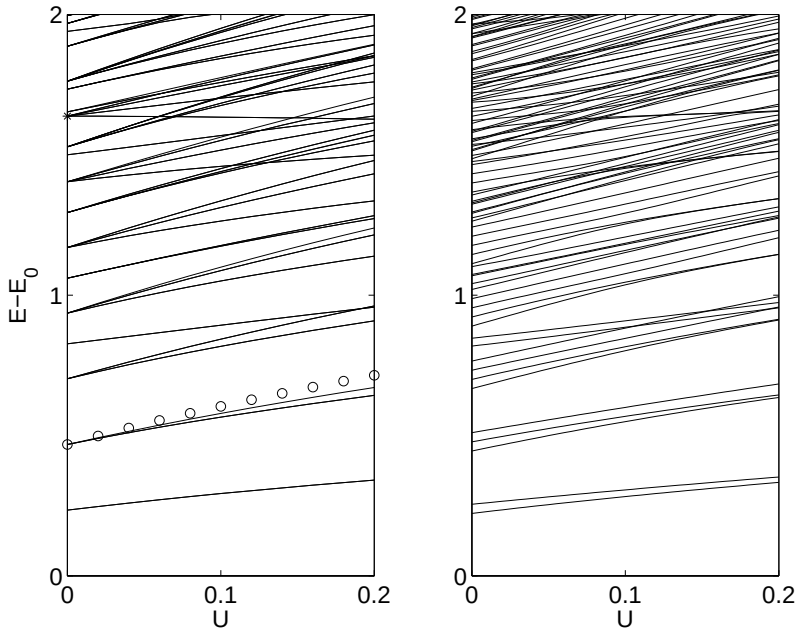

Figure 8. Low-energy levels of $N = 7$ atoms in a lattice with $L = 9$ sites for magnitude of the scattering potential $\epsilon = 0$ (left) and $\epsilon = 0.2$ (right). The state with supercurrent ($\kappa = 2\pi/L$) corresponds to the lowest level in the group of levels marked by an asterisk. Open circles corresponds to the quasiparticle energy $\hbar\omega_1$.

decrease of $Q = Q(U)$, seen in the figure, is due to population of the single-particle quasimomentum states with $\kappa \neq 0$, and is often referred to as the Bogoliubov depletion of the BEC. Additionally, the dashed and dash-dotted lines in Fig. 9 depict the overlap of the states $|\kappa = 2\pi/L\rangle$ and $|\kappa = 4\pi/L\rangle$ with the Bogoliubov states, originating from these supercurrent states, which we calculate by substituting the single-particle excitation energy $E_k = J[1 - \cos(2\pi k/L)]$ in Eq. (17) by

$$E_k = 0.5J[\cos(\kappa + 2\pi k/L) + \cos(\kappa - 2\pi k/L) - 2\cos\kappa] \sim (2\pi k/L)^2 \cos\kappa \,. \tag{26}$$

Finally, the series of dots correspond to the quantity (25). It is seen that for $\kappa = 0$ dots perfectly follow the solid continuous line. Thus the ground state of the system is indeed well approximated by the Bogoliubov state. With exception of two narrow avoided crossings this is also the case for the state of our interest $\kappa = 2\pi/L$. However, for higher initial quasimomentum $\kappa = 4\pi/L$, the Bogoliubov state is seen to be completely destroyed by the large number of avoided crossings.

5. Conclusions

Within the formalism of the Bose-Hubbard model we have considered time evolution of the atomic supercurrent in a ring optical lattice with weak on-site disorder. For vanishing atom-atom interactions, weak disorder induces Rabi oscillations of the atomic current, where the atoms periodically change their velocity to the opposite one. For non-vanishing atom-atom interactions, the supercurrent dynamics depend crucially on

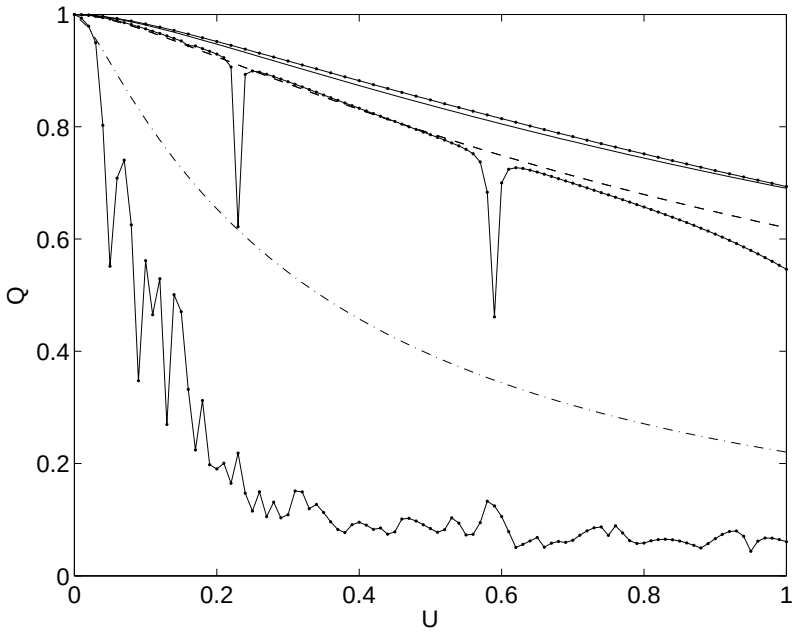

Figure 9. Overlap of the states $|\kappa = 0\rangle$ (solid line), $|\kappa = 2\pi/L\rangle$ (dashed line), and $|\kappa = 4\pi/L\rangle$ (dash-dotted line) with the Bogoliubov states, originating from these supercurrent states. Dots (guided by the solid lines) show the quantity (25), calculated for these three values of the initial quasimomentum. The system parameters are the same as in Fig. 8(a).

the initial quasimomentum κ (i.e., the initial velocity of the atoms). Namely, for a high quasimomentum $\kappa \sim \pi/2$ the supercurrent exponentially decays as the interaction constant U exceeds some critical value, while for a low quasimomentum $\kappa \ll \pi/2$ the oscillatory behaviour of the suppercurrent changes to a persistent current.

The explanation for these effects is found in the structure of low- and high-energy spectra of the Bose-Hubbard model. It is shown that the low-energy spectrum of the system is regular, and the positions of the energy levels can be found by using a Bogoliubov approach. In contrast, the high-energy spectrum shows a transition from regular to a chaotic one if U exceeds its critical value. Using the results of the random matrix theory, we show that this transition is reflected in the exponential decay of the supercurrent with the decay constant proportional to U^2.

This work was supported by Deutsche Forshungsgemeinschaft within the SPP1116 program.

[1] M. Greiner, O. Mandel, T. Esslinger, T. W. Hänsch, and I. Bloch, *Quantum phase transition from a superfluid to a Mott insulator in a gas of ultracold atoms*, Nature **415**, 39 (2002).

[2] D. Jaksch and P. Zoller, *The cold atom Hubbard toolbox*, Ann. Phys. **35**, 52 (2005).

[3] S. Kuhr, W. Alt, D. Schrader, M. Müller, V. Gomer, and D. Meschede, *Deterministic Delivery of a Single Atom*, Science **293**, 278 (2001).

[4] C. S. Chuu *et. al.*, *Direct observation of sub-poissonian number statistics in a degenerate Bose gas*, Phys. Rev. Lett. **95**, 260403 (2005).

[5] L. Amico, A. Osterloh, and F. Cataliotti, *Quantum many particle systems in ring-shaped optical*

lattices, Phys. Rev. Lett. **95**, 063201 (2005).

[6] R. Roth and K. Burnett, *Phase diagram of bosonic atoms in two-colour superlattices*, Phys. Rev. A **68**, 023604 (2003).

[7] L. D. Landau, J. Phys. USSR **5**, 71 (1941).

[8] G. E. Astrakharchik and L. P. Pitaevskii, *Motion of a heavy impurity through a BEC*, Phys. Rev. A **70**,013608 (2004).

[9] Biao Wu and Qian Niu, *Superfluidity of BEC in an optical lattice: Landau-Zener tunnelling and dynamical instability* New J. of Physics **5**, 104 (2003).

[10] S. Smerzi, A. Trombettoni, P. G. Kevrekidis, and A. R. Bishop, *Dynamical superfluid-insulator transition in a chain of weakly coupled BECs*, Phys. Rev. Lett. **89**, 170402 (2002).

[11] V. V. Konotop and M. Salerno, *Modulation instability in BECs in optical lattices* Phys. Rev. A **65**, 021602R (2002).

[12] L. Fallani, L. De Sarlo, J. E. Lye, M. Modugno, R. Saers, C. Fort, and M. Inguscio, *Observation of dynamical instability for a BEC in a moving 1D optical lattice*, Phys. Rev. Lett. **93**, 140406 (2004).

[13] F. S. Cataliotti, L. Fallani, F. Ferlaino, C. Fort, P. Maddaloni, and M. Inguscio, *Superfluid current disruption in a chain of weakly coupled BEC*, New J. of Phys. **5**, 71 (2003).

[14] R. G. Scott, A. M. Martin, S. Bujkiewicz, T. M. Fromhold, N. Malossi, O. Morsch, M. Cristiani, and E. Arimondo, *Transport and disruption of Bose-Einstein condensates in optical lattices*, Phys. Rev. A **69**, 033605 (2004).

[15] A. R. Kolovsky, *Dynamical instability, chaos, and Bloch oscillations of BECs in tilted optical lattices*, e-print: cond-mat/0412195.

[16] A. Polkovnikov, E. Altman, E. Demler, B. Halperin, and M. D. Lukin, *Decay of superfluid currents in a moving system of strongly interacting atoms*, Phys. Rev. A **71**, 063613 (2005).

[17] See, for example, chapter VII in review [18].

[18] A. J. Leggett, *BEC in the alkali gases: Some fundamental concepts*, Rev. of Mod. Phys. **73**, 307 (2001).

[19] A.R.Kolovsky and A.Buchleitner, *Quantum chaos in the Bose-Hubbard model*, Europhys. Lett. **68** (2004), 632.

[20] Y. V. Fyodorov, O. A. Chubykalo, F. M. Izrailev, and G. Casati, *Wigner random banded matrices with sparse structure: local density of states*, Phys. Rev. Lett. **76**, 1603 (1996).

[21] M. Hiller, T. Kottos, and T. Geisel, *Complexity in parametric Bose-Hubbard Hamiltonians structural analysis of eigenstates*, Phys. Rev. A, to appear.